Miner Petrol
DOI 10.1007/s00710-012-0254-2

ORIGINAL PAPER

# A contribution to the crystal chemistry of the voltaite group: solid solutions, Mössbauer and infrared spectra, and anomalous anisotropy

**Juraj Majzlan · Hannes Schlicht · Maria Wierzbicka-Wieczorek · Gerald Giester · Herbert Pöllmann · Beatrix Brömme · Stephen Doyle · Gernot Buth · Christian Bender Koch**

Received: 9 May 2012 / Accepted: 19 November 2012


**Abstract** Voltaite is a mineral of fumaroles, solfatares, coal-fire gas vents, and acid-mine drainage systems. The nominal composition is $K_2Fe_5^{2+}Fe_3^{3+}Al(SO_4)_{12}\cdot 18H_2O$ and the nominal symmetry is cubic, $Fd\bar{3}c$. The tetragonal ($I4_1/acd$) superstructure of voltaite is known as the mineral pertlikite. In this study, we investigated 22 synthetic voltaite samples in which $Fe^{2+}$ was partially or completely replaced by Mg, Zn, Mn, or Cd, by single-crystal and powder X-ray diffraction (both in-house and synchrotron). Two samples contained $NH_4^+$ instead of $K^+$. The structure of voltaite is based on a framework defined by kröhnkite-like heteropolyhedral chains which host both $M^{3+}$ and $M^{2+}$ in octahedral coordination. Unit cell dimensions of the end-members scale almost linearly with the size of $M^{2+}$. In the $Fe^{2+}$-Mg-Zn solid solutions, the $Fe^{2+}$-Mg and $Fe^{2+}$-Zn solutions are linear (ideal) in terms of their lattice-parameter variations. The Mg-Zn solid solution, however, is strongly non-ideal. A detailed analysis of the topology of the chains showed that this behavior originates in expansion and contraction of individual $M^{2+}$-O bonds within the chains. In the Mg-Zn solid solution, some of the $M^{2+}$-O bonds expand while none contract. In the other solid solutions, expansion of some $M^{2+}$-O bonds is always compensated by contraction of the other ones. Parts of the nominally cubic crystals are optically anisotropic and their symmetry is found to be tetragonal by single crystal X-ray diffraction measurements. The coexistence of cubic and tetragonal sectors within a single crystal without any detectable difference in their chemical composition is difficult to explain in terms of growth of such composite crystals. Mössbauer and infrared spectra collected on our synthetic crystals conform with previously published data.

Editorial handling: T. Armbruster

Dedicated to Prof. Josef Zemann on the occasion of his 90th birthday

**Electronic supplementary material** The online version of this article (doi:10.1007/s00710-012-0254-2) contains supplementary material, which is available to authorized users.

J. Majzlan (✉) · H. Schlicht · M. Wierzbicka-Wieczorek
Institute of Geosciences, Friedrich-Schiller-Universität Jena,
Burgweg 11,
07749 Jena, Germany
e-mail: Juraj.Majzlan@uni-jena.de

G. Giester
Institute of Mineralogy and Crystallography, Faculty of Geosciences, Geography and Astronomy, University of Vienna, Althanstr. 14,
1090 Vienna, Austria

H. Pöllmann · B. Brömme
Institute of Geosciences, Martin-Luther-Universität Halle-Wittenberg, Von-Seckendorff-Platz 4,
06099 Halle, Germany

S. Doyle · G. Buth
ANKA, Karlsruhe Institute of Technology,
Hermann-von-Helmholtz-Platz 1,
76344 Eggenstein-Leopoldshafen, Germany

C. Bender Koch
Department of Chemistry, University of Copenhagen,
Universitetsparken 5,
DK-2100 Copenhagen, Denmark

## Introduction

Voltaite was originally described as a mineral from fumaroles and solfatares in the volcanic field of southern Italy and named after the Italian physicist Alessandro Volta. Rammelsberg (1860) reported that the mineral was identified as early as 1792 by Breislak in Solfatana and later investigated by Scacchi and Dufrénoy. The relatively complex chemical composition was a reason for the early confusion and Rammelsberg

Published online: 05 December 2012

(1860) noted that the mineral "deserves further investigation". Other members of the voltaite group e.g., Tl-$Fe^{2+}$-voltaite, Tl-Mg-voltaite, Tl-Cd-voltaite, Rb-Cd-voltaite, $NH_4$-Mg-voltaite were reported by Gossner and Fell (1932); Rb-Mn, $NH_4$-Zn, Rb-Zn and Tl-Zn voltaite by Gossner and Drexler (1933) and K-Zn, Rb-Co, Rb-Mg and $NH_4$-Co voltaite by Gossner and Besslein (1934). The anomalous optical anisotropy and morphology of voltaite has been described by Gossner and Bäuerlein (1933). The magnetic properties and the distribution of iron ions in voltaite were investigated by Hermon et al. (1976) and Mössbauer spectroscopy was employed by Long et al. (1980). Optical characterization of voltaite crystals was reported by Beveridge and Day (1979).

The crystal structure of voltaite was solved by Mereiter (1972) who was also able to determine the precise nominal composition as $K_2M_5^{2+}M_3^{3+}Al(SO_4)_{12}\cdot 18H_2O$ where $M^{2+}$ is mostly Mg or $Fe^{2+}$ and $M^{3+}$ is mostly $Fe^{3+}$, with the nominal symmetry as cubic, space group $Fd\bar{3}c$. The cubic symmetry was obvious already to the early researchers as voltaite tends to form euhedral crystals with the octahedron as a dominant form.

The tetragonal superstructure of voltaite has been described by Ertl et al. (2008) as a new mineral pertlikite. The symmetry change from cubic ($Fd\bar{3}c$) to tetragonal ($I4_1/acd$) is a result of ordering of the divalent cations in the structure.

The formation of voltaite in fumaroles (Zavalia and Galliski 1995; Marquez-Zavalia et al. 2001) occurs via the same mechanisms which operate in man-made high-temperature gaseous streams, such as coal-fire gas vents (Stracher et al. 2005) or emissions from coal-fired power plants (Gieré et al. 2007). Voltaite is also well known in the context of acid mine drainage (Nordstrom and Alpers 1999; Jambor et al. 2000) where decomposition of pyrite releases metals, sulfate and acidity. Once formidable concentrations of these aqueous ions are attained, voltaite crystallizes from metal-rich sulfuric acid with very low pH values, for example at the Iron Mountain Superfund site, California (Nordstrom and Alpers 1999).

This study was sparked by our interest in the sulfate minerals in general and in particular the difficulties encountered during routine lattice parameter refinement of natural voltaite samples. The estimated standard deviations (e.s.d.'s) on the lattice parameters were always found to be one or two orders of magnitude worse than for the associated minerals, despite that the voltaite crystals appeared perfect and euhedral. The powder XRD peaks were not broadened, suggesting that the large e.s.d.'s are caused by structural inhomogeneity. Hence, the aim of this study was to synthesize a suite of voltaite samples, exploring the substitutions of metals (Zn, Mg, Mn, Cd, Cu, Ni) on the position of $Fe^{2+}$, and the substitution of $NH_4$ for K. Furthermore, solid solutions between the $Fe^{2+}$, Zn and Mg end-members were synthesized.

All samples were investigated by an X-ray diffraction method, either single-crystal or powder X-ray diffraction (XRD), using both in-house instruments and a synchrotron source. This was complemented by chemical analyses with inductively-coupled plasma optical emission spectrometry (ICP-OES), energy-dispersive X-ray spectrometry, and inspection of the products by polarized-light optical microscopy and reflection goniometry. We focused on the variation of cell parameters, interatomic distances and crystal morphology caused by the substitution of $Fe^{2+}$. The observation and analysis of anomalous anisotropy in cross-polarized light was also an important and intriguing part of our investigation. In addition, infrared and Mössbauer spectra were measured on selected samples.

For the purposes of this study, we adopt a notation which explicitly states the chemical composition of the voltaite samples studied. This notation is necessary because most samples deviate much from the nominal composition $K_2Fe_5^{2+}Fe_3^{3+}Al(SO_4)_{12}\cdot 18H_2O$. For the voltaite samples having K as the monovalent cation, only the divalent cation is specified, for example Zn-voltaite or Fe60Mg40-voltaite. The numerical coefficients specify the nominal atomic proportions of the cations on the divalent site. For the voltaite samples having ammonium ion as the monovalent cation, we also specify the presence of this ion, for example $NH_4$-Mn-voltaite.

## Syntheses and methods

### Syntheses

The syntheses of all samples were based on the method of Gossner and Arm (1930). After initial experiments with different mass ratios of starting chemicals, we could ascertain the optimal conditions for the growth of large single crystals of voltaite. The masses of the sulfates are listed in Tables 1 and 2. The starting chemicals were purchased from the supplier and used as received.

The reagents were weighed out and mixed in a beaker, dissolved in 30 mL of deionized water and acidified with 4.5 mL of 96 % sulphuric acid. The beaker was placed in a sand bath at 80 °C. We found it essential for a successful synthesis to mix the chemicals in cold water and heat the solution only after dissolution of the chemicals. Larger crystals formed if the beaker was covered with an aluminum foil only perforated at a few places to keep the evaporation rate low. The synthesis was finished after 72 to 96 h at 80 °C. After this time, the voltaite crystals ceased growing. The crystals were taken out from the remaining liquid. While still wet, the crystals were easily separated from most of the other phases present in the beaker. The crystals were then dried by wiping them with kimwipes. They were large enough to simply separate them from the other phases with a needle under a binocular microscope for the XRD experiments. Syntheses with $Cu^{2+}$ and $Ni^{2+}$ were also carried out but no voltaite was observed, either visually or by powder X-ray diffraction. The phases grown here were rhomboclase and probably various

**Table 1** Masses of sulfates used for the synthesis of the Fe-Mg-Zn voltaite samples. In addition, 0.67 g $K_2SO_4$, 2.85 g $Fe_2(SO_4)_3 \cdot 6H_2O$[a], and 3.91 g $Al_2(SO_4)_3 \cdot 17H_2O$ were added to all synthesis in this table

| Sample | $FeSO_4 \cdot 7H_2O$ [g] | $MgSO_4 \cdot 7H_2O$ [g] | $ZnSO_4 \cdot 7H_2O$ [g] | *a* (Å) | M[b] |
|---|---|---|---|---|---|
| Fe100 | 6.04 | | | 27.174(3) | |
| Mg100 | | 4.79 | | 27.0188(3) | 0 |
| Zn100 | | | 6.42 | 27.0276(3) | |
| Fe80Mg20 | 4.83 | 0.96 | | 27.1525(3) | |
| Fe60Mg40 | 3.62 | 1.92 | | 27.1275(5) | |
| Fe40Mg60 | 2.42 | 2.87 | | 27.1050(4) | 0.459 |
| Fe20Mg80 | 1.21 | 3.83 | | 27.0884(3) | |
| Fe80Zn20 | 4.83 | | 1.28 | 27.151(3) | |
| Fe60Zn40 | 3.62 | | 2.57 | 27.133(3) | 0.527 |
| Fe40Zn60 | 2.42 | | 3.85 | 27.108(3) | |
| Fe20Zn80 | 1.21 | | 5.14 | 27.090(3) | |
| Mg80Zn20 | | 3.83 | 1.28 | 27.036(3) | |
| Mg60Zn40 | | 2.87 | 2.57 | 27.042(3) | |
| Mg40Zn60 | | 1.92 | 3.85 | 27.036(3) | 0 |
| Mg20Zn80 | | 0.96 | 5.14 | 27.033(3) | |

Lattice parameter *a* is listed for each sample with the estimated standard deviation reported in the parentheses

[a] The starting material is reported here as $Fe_2(SO_4)_3 \cdot 6H_2O$. We have done a thermogravimetric analysis which showed that the composition is $Fe_2(SO_4)_3 \cdot \sim 5.5H_2O$. The problem is that this chemical is hygroscopic and even during longer weighing, one sees the mass increasing. Therefore, the composition $Fe_2(SO_4)_3 \cdot 6H_2O$ is probably the best representation of what was used

[b] The $Fe^{2+}/(Fe^{2+}+Fe^{3+})$ ratio determined by Mössbauer spectroscopy

simple divalent metal sulfates $MSO_4 \cdot nH_2O$. The latter ones were believed to be seen visually but there were so many XRD peaks that we did not follow these syntheses further.

## Methods

### *Optical microscopy*

For optical microscopy, we used standard thin sections or simply ground voltaite samples. The thin sections were prepared in all steps without using water-based solutions or suspensions, polishing or cleaning media, to avoid dissolution of voltaite. Voltaite crystals were also imaged and photographed with a Keyence microscope VHX-1000 with real-time image stitching.

### *Elemental analysis*

For the chemical analyses with ICP-OES, 100 mg of each sample was dissolved in 25 mL ultrapure water and acidified with 1 mL concentrated nitric acid. Of the resulting solution, 15 mL were retained and diluted prior to the analysis to a volume of 600 mL.

After optical microscopy, selected thin sections and individual crystals were coated with a thin carbon layer for further electron microscopy work. For energy-dispersive X-ray spectrometry (EDX), we used a Cameca SX-50 electron microprobe with an acceleration voltage of 20 kV and a current of 20 nA. Two types of analyses were performed. One was the standard point analysis with a counting time of 60 s. The other type were line analyses along pre-selected profiles, with a step of 1 μm and counting time of 2 s at each step. A scanning electron microscope (SEM) Zeiss ULTRA Plus was also used for EDX element mapping (20 kV, 20 nA) and to obtain high-resolution secondary electron images of individual crystals (5 kV, 20 nA).

### *Powder X-ray diffraction*

An initial check of all synthesis products was done on powdered samples with a powder X-ray diffractometer Bruker D8 ADVANCE with DAVINCI design, equipped with Cu X-ray source, Ni filter, and a Lynxeye 1D detector. The data were collected at room temperature, over angular range of 5° to 60° 2Θ, with step of 0.02° 2Θ, and counting time of 2 s per point.

Selected samples (Mg80Zn20, Fe40Mg60) were powdered and investigated at bending-magnet powder X-ray diffraction beamline PDIFF at the synchrotron light source ANKA (Angströmquelle Karlsruhe, Germany). X-rays of wavelength of 0.82694(1) Å were selected by a double crystal Si(111) monochromator. The wavelength and the zero angle of the diffractometer were determined with

**Table 2** Masses of sulfates used for the synthesis of the K-Fe, K-Mn, K-Cd, $NH_4$-Fe, and $NH_4$-Mn voltaite. Each of these samples contains only one divalent cation, the occupancies of the $M^{2+}$ sites are therefore not given

| Sample | $Fe_2(SO_4)_3 \cdot 6H_2O$ [g] | $Al_2(SO_4)_3 \cdot 17H_2O$ [g] | Additional chemicals [g] | Additional chemicals [g] | *a* (Å) | M[a] |
|---|---|---|---|---|---|---|
| Fe100A | 2.99 | 3.47 | $K_2SO_4$: 0.67 | $FeSO_4 \cdot 7H_2O$: 4.31 | 27.166(3) | |
| Mn100 | 2.62 | 3.35 | $K_2SO_4$: 0.69 | $MnSO_4 \cdot 7H_2O$: 3.38 | 27.270(3) | 0 |
| $NH_4$-Fe | 2.62 | 3.35 | $(NH_4)_2SO_4$: 0.46 | $FeSO_4 \cdot 7H_2O$: 4.84 | 27.239(3) | 0.633 |
| $NH_4$-Mn | 2.62 | 1.12 | $(NH_4)_2SO_4$: 0.46 | $MnSO_4 \cdot 7H_2O$: 3.38 | 27.394(3) | |
| Cd100 | 2.85 | 3.91 | $K_2SO_4$: 0.67 | $CdSO_4 \cdot 2.67H_2O$: 8.29 | 27.425(3) | |

Lattice parameter *a* is listed for each sample with the estimated standard deviation reported in the parentheses

[a] The $Fe^{2+}/(Fe^{2+}+Fe^{3+})$ ratio determined by Mössbauer spectroscopy

silicon (NIST standard reference material 640) powder. The sample was loaded into a 1.0 mm glass capillary which was rotated about its axis during the data collection. The intensity of the incoming beam was monitored during the data collection by an ion chamber and the measured intensities of the diffracted beam were corrected for the decay and fluctuations of the primary beam. The XRD patterns were collected at room temperature over an angular range of 4° to 40° 2Θ with step of 0.005°, and counting time of 1 s per point.

*Single-crystal X-ray diffraction*

To prepare the samples for single crystal X-ray diffraction, crystals of each sample were cut to a maximum size of 100 μm. We used a computer controlled Nonius Kappa diffractometer with APEX II detector and X-rays of wavelength of 0.71069 Å, generated by a molybdenum X-ray tube at 55 kV and 30 mA. The samples were measured at a temperature of 120 K, over an angular rage of 1° <Θ< 27.48°.

Single-crystal data for one selected sample Fe40Mg60 (with anomalous anisotropy) were collected at the bending-magnet beamline for single crystal diffraction (SCD) of the synchrotron facility ANKA in Karlsruhe (Germany). The incoming beam was monochromatized to a wavelength of 0:8000(1) Å by a Si(111) double-crystal monochromator. The sample crystal was mounted on a Bruker D8 diffractometer with fixed χ axis. Single crystal X-ray diffraction data were recorded with an APEX CCD detector at a distance of 50 mm and a 2θ angle of 32º, corresponding to a resolution of 0.74 Å.

The single crystal XRD data were treated with the SHELX programs of Sheldrick (2008). The starting model for the refinements was the structure of voltaite described by Mereiter (1972). All crystal data and details of the structure refinement were submitted in a tabular form as supplementary information (Tables S0–32) and as CIF files to the ICDD database.

*Mössbauer and infrared spectroscopy*

Mössbauer spectra were obtained at room temperature and 80 K using a conventional constant acceleration spectrometer with a $^{57}$Co in Rh source. The spectrometer was calibrated using a 12.5 μm foil of natural Fe at room temperature and isomer shifts are given with respect to the center of the spectrum of this sample. The samples were prepared as thin samples and no thickness corrections were applied. Fitting of the paramagnetic spectra were carried out using simple Lorentzian shaped doublets that were constrained to have identical lines in complex spectra. The experimental line width of the instrument is 0.22 mm·s$^{-1}$.

The Fourier-transform infrared (FTIR) spectra were recorded as KBr pellets in the region of 400 to 4,000 cm$^{-1}$ using a Nicolet Avatar 370 DTGS (ThermoElectron).

## Results and discussion

### Color and morphology

The substitutions of the divalent metals modified the color and morphology of the voltaite crystals. Voltaite with any amount of $Fe^{2+}$ is dark green and translucent on thin edges and the crystals appear to be black (Fig. 1a). Crystals in which $Fe^{2+}$ is completely replaced by Zn, Mg, or Cd are yellow (Fig. 1b). Complete substitution of $Fe^{2+}$ by $Mn^{2+}$ causes a deep red-orange color (Fig. 1c). Tiny white needles were associated with some of the $Fe^{2+}$-containing voltaite crystals. These needles were too small for diffraction analyses, but they are most likely crystals of halotrichite. The size of the voltaite crystals varied between 0.5 and 3 mm. Voltaite and halotrichite crystals formed always on the top of a grayish-green substrate. According to the powder XRD data, the substrate is a mixture of rhomboclase, $(H_5O_2)Fe(SO_4)_2{\cdot}2H_2O$, and the phase $(H_3O)Fe^{3+}(SO_4)_2$ (Peterson et al. 2009).

The morphology of the obtained crystals is simple and consists of one to three cubic forms. Zn- and Mg-voltaite show simple hexahedral forms, the pure $Fe^{2+}$-voltaite forms octahedra. Mixed compositions along the Fe-Zn and Fe-Mg join have more complex shape. The angles between the faces on these crystals were measured by reflection goniometry. The polar and azimuthal angle ρ and ϕ are nearly identical for both measured crystals. The crystals show 26 faces (6 hexahedral faces, 8 octahedral faces and 12 rhombododecahedral faces) with varying dominance (Fig. 1d). The rhombododecahedral {110} faces and hexahedral {100} faces become more prominent with the increasing Mg-content. The morphology of the voltaite crystals as a function of their composition is summarized in Fig. 2.

### Optical microscopy

The nominally cubic symmetry of voltaite implies that the crystals should appear dark in cross-polarized light. In contrast with this expectation, most samples contain anisotropic sectors of variable and striking shape. As the thin sections allow only for two-dimensional observations within the plane of the sections, a reconstruction of the geometry of the sectors is difficult. Within some crystals, the sectors appear to be constrained by four- or three-fold symmetry along the rotation axes in the crystal (Fig. 3a). These sectors are situated in the external portion of the crystals, with a

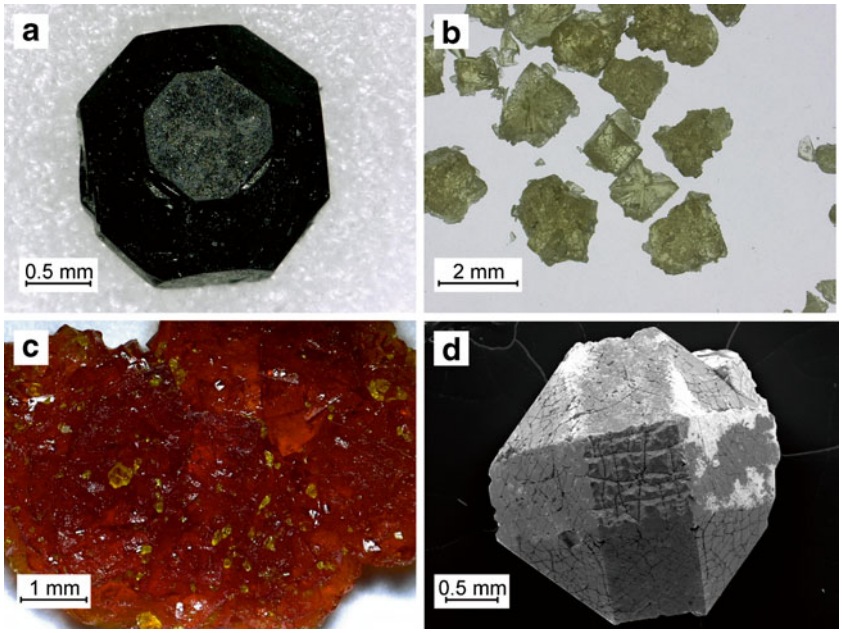


**Fig. 1** Optical microphotographs of **a** Fe80Mg20-voltaite, **b** Mg20Zn80-voltaite, **c** Mn100-voltaite. Note the color variations as described in text. **d** SEM image of Fe60Mg40-voltaite showing the combination of hexahedral, octahedral, and rhombododecahedral faces

sharp border between the cubic and non-cubic portions of the crystals. A weak undulation of bright and less bright bands parallel to the interface of the anisotropic sector and isotropic body of the crystal was observed. Other crystals contain sectors with four-fold symmetry but their interface is not as sharp as before (Fig. 3b). They attach to the isotropic body along several interfaces, giving these interfaces a curved appearance. Similar sectors, but with weaker anisotropy, were observed in sample Mn100 (Fig. 3c). However, in this sample additional anisotropic portions can be seen. These are lamellae radiating from the center of the crystal. Other crystals contain only such lamellae and no sectors with visible symmetry (Fig. 3d).

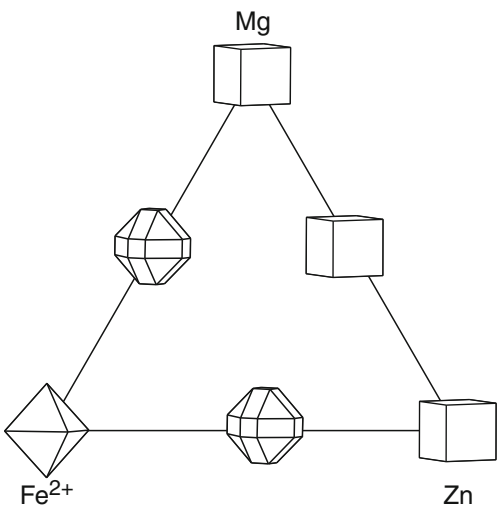


**Fig. 2** A schematic triangular diagram with the morphology of the crystals synthesized in this study

## Mössbauer spectroscopy

Mössbauer spectra of the selected voltaite samples show one or two doublets (see Table 3, Fig. 4). If only one doublet is present, it is centered at δ ~0.47 mm·s$^{-1}$ and assigned to ferric iron in the samples. These results confirmed that the samples which are not black contain only $Fe^{3+}$. If $Fe^{2+}$ is present, another doublet, centered at δ = 1.22–1.26 mm·s$^{-1}$ appears. These data agree well with Mössbauer parameters from natural samples, although some of the natural samples must be fitted with three doublets (Majzlan et al. 2011). Two of these doublets can be assigned to $Fe^{2+}$, suggesting that in these voltaite crystals, $Fe^{2+}$ is found in two distinct environments. An alternative explanation of the second $Fe^{2+}$ doublet would be an impurity in our samples, possibly a phase from the halotrichite group. The large voltaite crystals, however, were easily separated from the rest of the material. The explanation of the second $Fe^{2+}$ doublet with an impurity gains weight by the finding that in case of pertlikite (Ertl et al. 2008), no additional $Fe^{2+}$ doublet is seen despite the three different Fe-bearing sites, if one accepts the partial tetragonal ordering of Fe/Mg as being no artifact.

## Elemental analyses

The data of the wet-chemical (ICP-OES) analyses for the voltaite solid solutions were re-calculated to 12 S atoms and the results are listed in Table 4. The measured Fe content was converted to $Fe^{2+}$ and $Fe^{3+}$ with the condition of electroneutrality for the structure. The calculations show analytical errors of 5–10 % which are apparent for the Mg-Zn solid solutions which do not contain any $Fe^{2+}$. The absence of $Fe^{2+}$ in these crystals was confirmed by Mössbauer spectroscopy and is

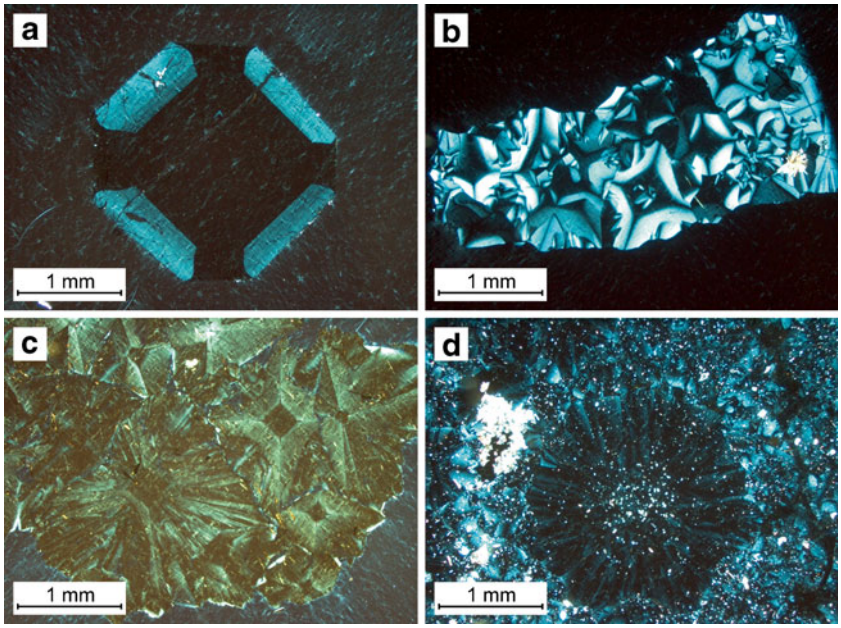


**Fig. 3** Optical microphotographs of thin sections of voltaite crystals (crossed polarizer). **a** Fe60Zn40-voltaite, **b** Mg80Zn20-voltaite, **c** Mn100-voltaite, **d** Zn100-voltaite

indicated by their light color. Furthermore, the calculated values always erroneously overestimate $Fe^{2+}$. The $Fe^{2+}/(Fe^{2+}+Fe^{3+})$ ratios from the elemental analyses agree within the 5–10 % margin with the values from Mössbauer spectroscopy. Keeping these analytical errors in mind, Table 4 represents the fractions of divalent metals in our voltaite samples.

The analytical results allow to deduce qualitative conclusions about the distribution of divalent metals between the aqueous solution and voltaite crystals. Semiquantitative or quantitative inferences are difficult to make, not only because of the analytical errors, but also because of the presence of the fine white needles, probably a solid solution of halotrichite-pickeringite, $(Fe^{2+},Mg)Al_2(SO_4)_4{\cdot}22H_2O$, in the product. Rhomboclase and $(H_3O)Fe(SO_4)_2$, both sulfates containing only $Fe^{3+}$, do not affect the ratios of the divalent cations in voltaite.

In both $Fe^{2+}$-Zn and $Fe^{2+}$-Mg solid solutions, the voltaite crystals show distinctly stronger preference for Zn and Mg, respectively. In the Mg-Zn solid solution, the crystals preferentially incorporated Mg over Zn. From this limited data set, it appears that voltaite accepts more readily $Mg^{2+}$ and $Zn^{2+}$ with closed electron shells, disfavors $Fe^{2+}$, and rejects $Ni^{2+}$ or $Cu^{2+}$, perhaps because the transition metal cations with incompletely filled *d* orbitals introduce too much anisotropy and hence strain into the tightly knitted heteropolyhedral network.

## Crystal structure of voltaite—general features

The crystal structure of voltaite was solved by Mereiter (1972). The structure is a tightly knitted heteropolyhedral network with cavities. The central feature of the structure is pinwheels

**Table 3** Mössbauer parameters of the voltaite samples at 295 K

| Sample | Fe(III) | | | | Fe(II) | | | |
|---|---|---|---|---|---|---|---|---|
| | δ ($mm{\cdot}s^{-1}$) | $\Delta E_Q$ ($mm{\cdot}s^{-1}$) | Γ ($mm{\cdot}s^{-1}$) | A (%) | δ ($mm{\cdot}s^{-1}$) | $\Delta E_Q$ ($mm{\cdot}s^{-1}$) | Γ ($mm{\cdot}s^{-1}$) | A (%) |
| Fe60Zn40 | 0.474 | 0.293 | 0.304 | 47.3 | 1.293 | 1.709 | 0.321 | 52.7 |
| Fe40Mg60 | 0.472 | 0.319 | 0.356 | 54.1 | 1.290 | 1.689 | 0.355 | 45.9 |
| $NH_4$-Fe | 0.452 | 0.382 | 0.293 | 36.7 | 1.312 | 1.819 | 0.338 | 63.3 |
| Mn100 | 0.467 | 0.286 | 0.313 | 100 | | | | |
| Mg40Zn60 | 0.475 | 0.321 | 0.519 | 100 | | | | |
| Mg100 | 0.467 | 0.318 | 0.398 | 100 | | | | |

δ is the isomer shift, $\Delta E_Q$ is the quadrupole splitting, $\Gamma$ is the line width, and $A$ is the spectral area

Uncertainties are better than 0.05 $mms^{-1}$ and areas better than 2 %. Note that the values of δ, $\Delta E_Q$, and Γ are reported to three decimal digits to highlight the minute differences between the samples

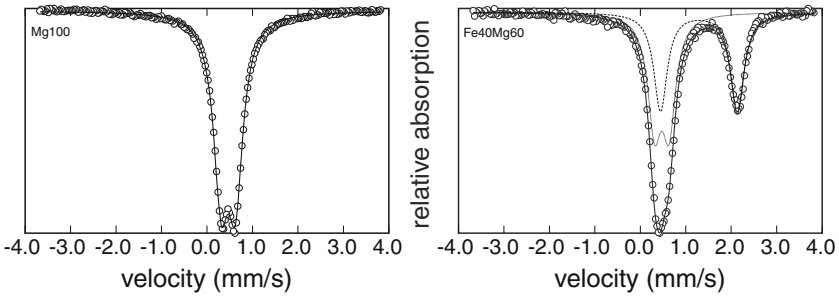


**Fig. 4** Mössbauer spectra of selected voltaite samples, marked with the sample codes (see Tables 1 and 2). The *thick solid lines* represent the fits to the experimental data. In b the *thin line* represent the Fe(III) component and the *dashed line* the Fe(II) component

centered at the $M^{3+}O_6$ octahedra, where $M^{3+}$ is mostly $Fe^{3+}$ (see further below). The site symmetry of $M^{3+}$ is $\bar{3}$ and all six ligands of $M^{3+}$ bridge the central cations to the adjacent $S^{6+}$ cations (Fig. 5). Each $M^{3+}$ position is a point in the structure where three heteropolyhedral chains intersect. The orientation of these chains is <1-10> (i.e., [1-10], [10$\bar{1}$], and [01$\bar{1}$]) and short fragments of all three are visible in Fig. 5. Figure 6 shows a longer portion of a chain, with its ladder-like arrangement of the $M^{2+}O_4(H_2O)_2$ octahedra and $SO_4$ tetrahedra. A larger slab with one system of these chains is shown in Fig. 7.

Such chains are also known from other structures, e.g. kröhnkite, $Na_2Cu(SO_4)_2(H_2O)_2$ (Dahlman 1952). The chain type is abundant in a number of sulfates, phosphates, arsenates, chromates, or molybdates with heteropolyhedral chains or layers, and these chains are then called the kröhnkite-type chains (Fleck et al. 2002). An example of a phosphate mineral with such chains is collinsite, $Ca_2(Mg,Fe)(H_2O)_2(PO_4)_2$, and an arsenate example is roselite, $Ca_2(Co,Mg)(H_2O)_2(AsO_4)_2$. Voltaite differs from all these minerals in that the chains in voltaite are not linked to each other only via hydrogen bonds and large polyhedra around cations such as $Ca^{2+}$, $K^+$, or $NH_4^+$ with high coordination numbers. In voltaite, the three chain systems are interwoven into a framework.

The spaces between the chains are occupied by $K^+$ or $NH_4^+$ cations in twelve-fold coordination (Fig. 7). The systems of chains create additional cavities which house disordered $Al(H_2O)_6$ octahedra. These octahedra connect to the rest of the structure only via hydrogen bonds.

Most cations are located at special positions: $K^+$ or $NH_4^+$ at 32*b* (1/4,1/4,1/4), $M^{3+}$ at 32*c* (0,0,0), $M^{2+}$ at 96*g* (1/4,y,$\bar{y}$), and $Al^{3+}$ at 16*a* (1/8,1/8,1/8). $S^{6+}$ and $H^+$ are found in general positions. Most of the oxygen atoms are also located at general positions, with the exception of one disordered $H_2O$ molecule which coordinates $Al^{3+}$. The H atoms of the disordered $H_2O$ molecules were not located.

## Crystal structure of cubic end-members

### *Mixing of $M^{2+}$ and $M^{3+}$ over the octahedral sites*

The nominal composition $K_2M_5^{2+}M_3^{3+}Al(SO_4)_{12}\cdot 18H_2O$ implies a strict distribution of the divalent and trivalent cations over the available 32*c* and 96*g* sites. Refinements of the end-member voltaite samples disproved this assumption. Similar site-distribution refinements were not possible for the Fe-, Mn-, and Zn-voltaite where the differences

**Table 4** Results of chemical analyses of the voltaite solid solutions, normalized to 12 S

| Sample | K | Al | Fe | Mg | Zn | $Fe^{2+}$ | $Fe^{3+}$ | I[a] | M[b] | Composition[c] |
|---|---|---|---|---|---|---|---|---|---|---|
| Mg80Zn20 | 2.009 | 1.234 | 3.137 | 3.434 | 1.115 | 0.220 | 2.917 | 0.070 | | $Mg_{0.755}Zn_{0.245}$ |
| Mg60Zn40 | 2.019 | 1.215 | 3.144 | 2.508 | 2.117 | 0.345 | 2.799 | 0.110 | | $Mg_{0.542}Zn_{0.458}$ |
| Mg40Zn60 | 1.972 | 1.225 | 3.039 | 1.679 | 3.057 | 0.234 | 2.805 | 0.077 | 0 | $Mg_{0.355}Zn_{0.645}$ |
| Mg20Zn80 | 2.020 | 1.201 | 3.082 | 0.843 | 3.981 | 0.519 | 2.563 | 0.168 | | $Mg_{0.175}Zn_{0.825}$ |
| Fe80Zn20 | 2.239 | 1.045 | 7.200 | 0.002 | 0.792 | 4.562 | 2.637 | 0.634 | | $Fe_{0.852}Zn_{0.148}$ |
| Fe60Zn40 | 2.133 | 1.024 | 6.600 | 0.002 | 1.545 | 4.099 | 2.501 | 0.621 | 0.527 | $Fe_{0.726}Zn_{0.274}$ |
| Fe40Zn60 | 2.200 | 1.053 | 5.522 | 0.002 | 2.576 | 3.079 | 2.442 | 0.558 | | $Fe_{0.545}Zn_{0.455}$ |
| Fe20Zn80 | 2.061 | 1.082 | 4.511 | 0.002 | 3.699 | 2.242 | 2.268 | 0.497 | | $Fe_{0.377}Zn_{0.623}$ |
| Fe80Mg20 | 2.561 | 0.969 | 7.233 | 0.500 | 0.001 | 4.171 | 3.062 | 0.577 | | $Fe_{0.893}Mg_{0.107}$ |
| Fe60Mg40 | 2.146 | 1.038 | 6.457 | 1.523 | 0.001 | 3.678 | 2.779 | 0.570 | | $Fe_{0.707}Mg_{0.293}$ |
| Fe40Mg60 | 2.224 | 1.060 | 5.602 | 2.287 | 0.001 | 2.785 | 2.817 | 0.497 | 0.459 | $Fe_{0.549}Mg_{0.451}$ |
| Fe20Mg80 | 2.421 | 1.013 | 4.971 | 2.767 | 0.001 | 1.907 | 3.064 | 0.384 | | $Fe_{0.408}Mg_{0.592}$ |

[a] The $Fe^{2+}/(Fe^{2+}+Fe^{3+})$ ratio determined from the ICP-OES

[b] The $Fe^{2+}/(Fe^{2+}+Fe^{3+})$ ratio determined by Mössbauer spectroscopy

[c] The stoichiometry of divalent cations, calculated from the ICP-OES data and normalized to 1 cation

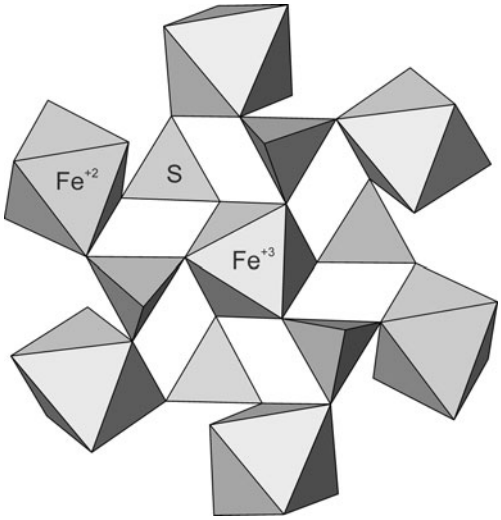


**Fig. 5** The pinwheel in the structure of voltaite projected onto (111) constructed by the central $M2O_6$ octahedron and six sulfate tetrahedra. Sulfate tetrahedra are white and hatched, $M1\phi_6$ octahedra are *grey*, and the $M2O_6$ octahedra are *white* and hatched with *dotted lines*

between the atomic number for the divalent metals are too small. On the other hand, refinement of Cd- and Mg-voltaite (samples Cd100, Mg100, see Table 1 for their lattice parameters) showed consistently a fraction of $M^{2+}$ on the nominal $M^{3+}$ site and vice versa. In the Mg-voltaite (two samples refined), the 32*c* (0,0,0) site was populated by ~75 % $Fe^{3+}$ and~25 %$Mg^{2+}$. The 96*g* (1/4,y,$\overline{y}$) site had ~80 %$Mg^{2+}$ and ~20 % $Fe^{3+}$. The oxidation state of Fe for one Mg-voltaite sample was confirmed by Mössbauer spectroscopy. The light yellowish color of the other Mg-voltaite sample suggests also fully trivalent state of Fe there. A similar situation was encountered in the Cd-voltaite. The 32*c* (0,0,0) site was occupied by ~60 % Fe and ~40 % Cd while the 96*g* (1/4,y,-y) site hosted ~40 % Fe and ~60 % Cd.

A similar information can be obtained for all voltaite samples by considering the refined M-O distances. Ideally,

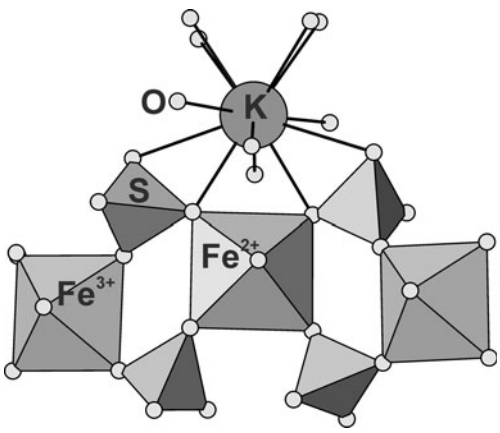


**Fig. 6** A short segment of the heteropolyhedral (kröhnkite-like) chains. The M1, M2, and $S^{6+}$ polyhedra shown by a polyhedral model like in Fig. 5, the $K^+$ polyhedra by a ball-and-stick model

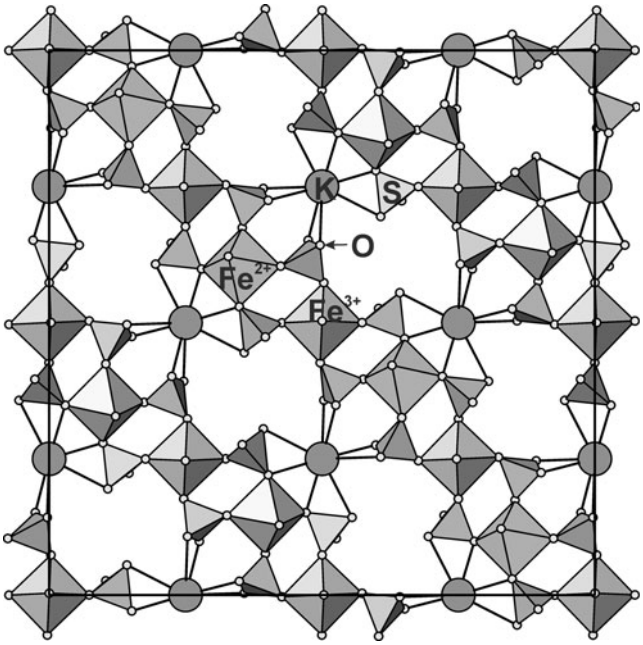


**Fig. 7** Projection of a slab from the voltaite structure onto (100). The kröhnkite-like chains extent diagonally across the unit cell in this projection. The M1, M2, and $S^{6+}$ polyhedra shown by a polyhedral model like in Fig. 5, the $K^+$ polyhedra by a ball-and-stick model

they should represent a linear combination of the individual M-O (e.g., $Fe^{2+}$-O, Zn-O, etc.) distances and therefore should reveal the occupancies of the M sites. We took the ionic radii for the di- and trivalent metals (all in octahedral coordination, high-spin state if applicable) and $O^{2-}$ (1.36 Å for three-fold coordination) from Shannon (1976). The calculations show that mixing of divalent and trivalent cations occurs in all voltaite samples. At the nominal $M^{3+}$ site, the smallest degree of mixing is observed in Fe-voltaite (~10 % $Fe^{2+}$ at this site). There is more mixing in Mg- and Zn-voltaite (~30 % of Mg or Zn at this site) and plenty of mixing in Mn- or Cd-voltaite (~50 % of $Mn^{2+}$ or Cd at this site). At the nominal $M^{2+}$ site, the bond-length calculations indicate consistently high degree of mixing, with 30–50 % of $Fe^{3+}$ at this site. We note that we did not constrain these calculations with the requirement of charge sum at the two sites and therefore the results should be considered semi-quantitative. However, taken together with the actual refinements for the Mg- and Cd-voltaite they demonstrate, that mixing of the di- and trivalent cations in the structure of voltaite is common.

*Lattice parameters*

The lattice parameters of the potassium-bearing end-members vary almost linearly with the ionic radii of the divalent cations (Fig. 8). The presence of ammonium expands the unit cell of voltaite slightly, as shown in Fig. 8. As for the potassium end-members, the unit cell of

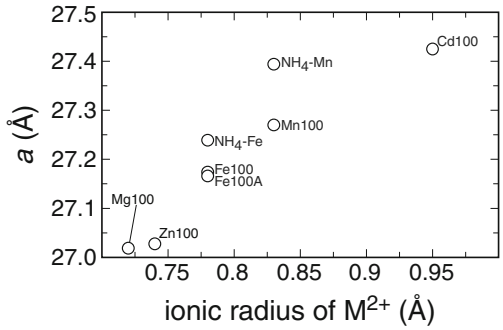


**Fig. 8** Variations of the lattice parameter *a* as a function of the ionic radius of $M^{2+}$

the ammonium end-members expands with the size of the divalent cation.

Crystal structure of cubic solid solutions among Fe-, Mg-, and Zn-voltaite

*Lattice parameters*

The variations of the lattice parameters in the three solid solutions are plotted in Fig. 9. Two different types of behavior can be seen. Mixing in the Mg-$Fe^{2+}$ and Zn-$Fe^{2+}$ solid solutions results in an almost linear variation of the lattice parameters. On the other hand, mixing in the Mg-Zn solid solution is strongly non-linear, with a distinct positive deviation for the intermediate members. Such behavior is surprising given that Mg and Zn have similar ionic radii (0.72 and 0.74 Å, respectively) which are different from the ionic radius of $Fe^{2+}$ (0.78 Å). The variations in the lattice parameters are caused by variations of the repeat distance of the kröhnkite-like chains.

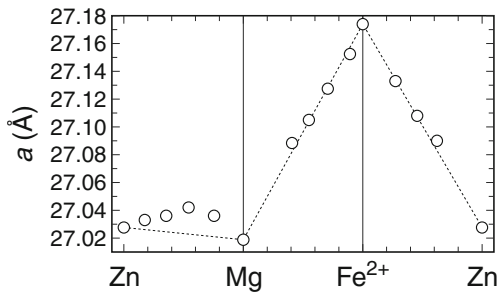


**Fig. 9** Variations of the lattice parameter *a* in the Zn-Mg, Mg-$Fe^{2+}$, and $Fe^{2+}$-Zn solid solutions. The errors are smaller than the symbol size. The *dashed line* connects the data for end-members and serves as a guide to the eye to judge the deviations from an ideal behavior. On the horizontal axis, the end-member compositions are marked with the symbol of the $M^{2+}$ cation. The ticks between the end-member compositions show the molar ratios $M_1^{2+}/(M_1^{2+}+M_2^{2+})$ [e.g., Zn/(Zn + Mg)] in the solid solutions. Note that the compositions used for plotting are the actual chemical compositions of the samples (cf. Table 4), not the nominal compositions. That is why the points do not necessarily appear to be equally spaced in their chemical composition

*Variations in the geometry of the coordination polyhedra*

The following section presents the variations in geometrical parameters of the polyhedra in the voltaite structure. These are the sulphate tetrahedra $SO_4$, M1 octahedra $M1O_4(H_2O)_2$, and the M2 octahedra $M2O_6$. The M1 polyhedra mostly house divalent cations ($M^{2+}$) and will be hereafter denoted as $M1\phi_6$, where $\phi$ is a ligand ($\phi = O^{2-}$ or $H_2O$). The M2 polyhedra are mostly centered on a trivalent ($M^{3+}$) cation.

We report and discuss the average bond length (<*c*-O>), where *c* is a cation, either $S^{6+}$, M1, or M2. We recall that the M1 and M2 positions are not occupied exclusively by a di- and trivalent cation, respectively. The <O-O> variable is the mean of the distances between the ligands in a polyhedron. In addition, we present two distortion indices: bond-length distortion parameter (BLDP) and edge-length distortion parameter (ELDP), as introduced by Griffen and Ribbe (1979). Both are defined as

$$\mathrm{BLDP} = \frac{1}{\langle c\text{–}O\rangle}\left[\frac{\sum^{x}(c\text{–}O - \langle c\text{–}O\rangle)^2}{x-1}\right]^{\frac{1}{2}}$$

$$\mathrm{ELDP}\,\frac{1}{\langle O\text{–}O\rangle}\left[\frac{\sum^{y}(O\text{–}O - \langle O\text{–}O\rangle)}{y-1}\right]^{2\,\frac{1}{2}}$$

where $x$=4 and $y$=6 for tetrahedra (for 4 *c*-O and 6 O-O distances, respectively) and $x$=6 and $y$=15 for octahedra (for 6 *c*-O and 15 O-O distances, respectively).

These parameters are measures of deviations of the individual atom-atom distances from a mean. BLDP is not considered further because this parameter was found to vary erratically for the $M1\phi_6$ octahedra and $SO_4$ tetrahedra. For the $M2O_6$ octahedra, BLDP is zero by symmetry constraints.

*Sulfate tetrahedra*

The least variable polyhedra in the structures of our voltaite samples are the sulfate tetrahedra (Fig. 10a, b). The <S-O> bond lengths vary in a narrow interval between 1.470 and 1.474 Å, typical for sulfates (cf. Hawthorne et al. 2000). The <O-O> distances in the sulfate tetrahedra also show little variation. Small changes are detected in both <S-O> and <O-O> distances and they are probably related to the adjustments of the sulfate tetrahedra as a response to the variable size of the $M^{2+}\phi_6$ octahedra within the heteropolyhedral chains.

*M1$\phi_6$ octahedra*

The variations of the <M1-O> bond lengths are shown in Fig. 10c. In the Mg-Zn-voltaite solid solution, the <M1-O> bond lengths deviate positively from a linear trend, with excess <M1-O> distances of 0.002 to 0.004 Å. These excess

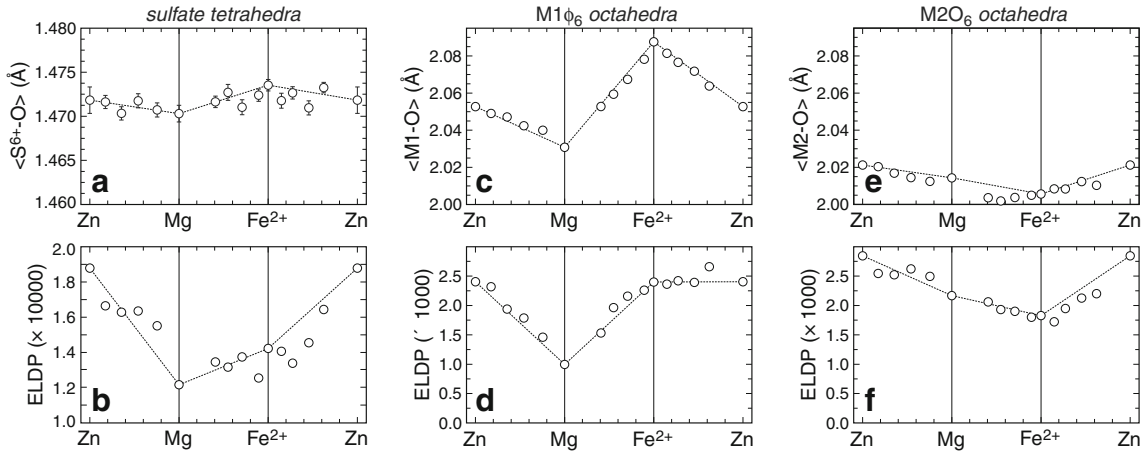


**Fig. 10** Diagrams showing the variations of the mean cation-oxygen (**a**, **c**, **e**) distances and the edge-length distortion parameters (ELDP) (**b**, **d**, **f**) for the sulfate tetrahedra (**a**, **b**), M1$\phi_6$ octahedra (**c**, **d**), and M2$O_6$ octahedra (**e**, **f**). For the distances, errors are shown if smaller than the symbol size. The *dashed lines* connect the data for end-members and serve as guides to the eye to judge the deviations from an ideal behavior. Note that the data for the M1$\phi_6$ and M2$O_6$ octahedra are shown with the same vertical scales for an easier comparison. For the definition of ELDP and further details, see text. The horizontal axes are labeled as in Fig. 9

lengths could be regarded as the reason for the excess lattice parameters in this solid solution. In the $Fe^{2+}$-Mg voltaite solid solution, however, the <M1-O> distances show a negative deviation of −0.002 to −0.004 Å from linearity but the lattice parameters vary almost linearly. In the $Fe^{2+}$-Zn voltaite solid solution, both the <M1-O> distances and the lattice parameters vary almost linearly between the end-members. Therefore, the <M1-O> distances alone cannot explain the trends seen in Fig. 9.

To rationalize the expansion and contraction of the unit cell, one can inspect the individual M1-O distances in a graph of the chain (Fig. 11b). There are three crystallographically independent distances in the M1 octahedra, these octahedra having the composition M1$(O2)_2(O4)_2(OW5)_2$. Of the three pairs of ligands, only O2 and O4 participate in the bonding within the chain, the OW5 position is a $H_2O$ molecule not involved in connecting polyhedra in the chains. The O2 atom is coordinated by the $S^{6+}$ and M1 cations and receives one hydrogen bond. The O4 atom is bonded to the $S^{6+}$, M1, and $K^+$ atoms. Because of the coordination environments, the M1-O4 bonds are always longer than the M1-O2 bonds. In the $Fe^{2+}$-Zn and $Fe^{2+}$-Mg solid solutions, the M1-O4 bonds deviate positively from linearity (i.e., they are longer than expected if the variations were linear) (Fig. 11a). Simultaneously, the M1-O2 bonds deviate negatively (i.e., they shorten). The magnitude of M1-O4 expansion (max. +0.005 Å) is smaller than the magnitude of M1-O2 contraction (max. −0.020 Å). It appears that the simultaneous expansion and contraction of the bonds within the M1$\phi_6$ polyhedron results in a near-linear variation of the chain repeat distance and hence the lattice parameters. On the other hand, the Mg-Zn octahedra experience expansion of the M1-O4 bonds but no contraction of the M1-O2 (Fig. 11a). Hence, the Mg-Zn octahedra expand non-linearly and this feature accounts for the positive, non-linear variation of the lattice parameters. The reasons for this behavior are difficult to comprehend.

A look at the ELDP values for the M1 octahedra (Fig. 10d) discloses a few more facts about them. The most regular arrangement of the ligands is encountered when the divalent cation is $Mg^{2+}$. Both $Fe^{2+}$ and $Zn^{2+}$ distort the octahedra in a similar fashion. These variations, however, do not explain why is only the Mg-Zn solid solution non-ideal.

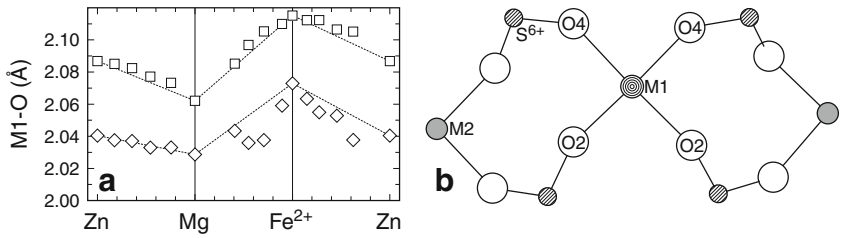


**Fig. 11** **a** Variations of the M1-O2 (*diamonds*) and M1-O4 (*squares*) bond distances in the Zn-Mg, Mg-$Fe^{2+}$, and $Fe^{2+}$-Zn solid solutions. The horizontal axis is labeled as in Fig. 9. **b** A graph of a heteropolyhedral chain with labeled atoms, showing the arrangement of the M1, O2, and O4 atoms within the chain

*$M2O_6$ octahedra*

The interatomic distances and ELDP for the $M2O_6$octahedra are shown in Fig. 10e and f. Here, we should note that all M2-O distances are identical, and therefore <M2-O> = M2-O. If any deviations from linear trends are present, they are negative. The M2-O bond lengths deviate slightly in the Mg-Zn solid solution and substantially in the Mg-$Fe^{2+}$ solid solution. The data shown in Fig. 10e and f can be rationalized if we consider the actual population of the M2 sites. As explained above, the nominal M2 sites are occupied by ~10 % $Fe^{2+}$ and ~90 % $Fe^{3+}$ in Fe-voltaite, but by ~30 %Mg or Zn and ~70 % of $Fe^{3+}$ in the Mg- or Zn-voltaite. In other words, the smallest degree of mixing is seen in the Fe-voltaite. Because the divalent cations are all larger than $Fe^{3+}$, the octahedra with the smallest fraction of the divalent cations can be expected to be the smallest, just as the data show. In addition, the smallest degree of mixing results in the smallest degree of distortion (cf. Fig. 10f). If we accept this explanation of the M2-O variations, it is interesting to note that there is very limited mixing not only the end member Fe-voltaite, but also throughout the $Fe^{2+}$-Mg solid solution.

Tetragonal superstructure of voltaite—structure of pertlikite

Our crystal of pertlikite was cut from a crystal of the Fe40Mg60-voltaite sample and was checked for its optical anisotropy before collecting the single-crystal diffraction data. Its tetragonal symmetry was confirmed and neither single-crystal XRD nor powder XRD data, both collected at a synchrotron source, showed any other deviation than cation ordering from the parent voltaite structure. We were looking for peak splitting or systematic variations in the peak widths in the synchrotron powder XRD data (Fig. 12) but found no indications that the anisotropy is caused by a mechanism other than cation ordering.

The refinement of the occupancies showed that the $M^{3+}$ site houses only Fe, based on the $M^{3+}$-O distances

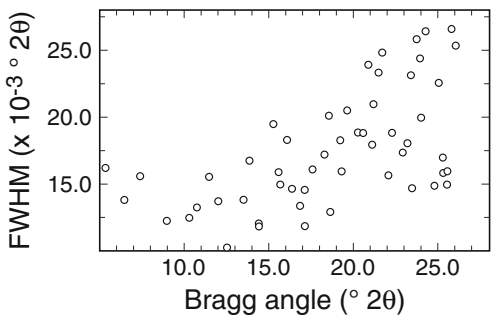


**Fig. 12** Full width at half-maximum (FWHM) of the powder X-ray diffraction peaks measured from synchrotron powder XRD data of the Mg80Zn20 sample

$Fe^{3+}$. Such occupancy is in agreement with the cubic portion of the sample Fe40Mg60 where the $M^{3+}$ site has also only $Fe^{3+}$. The two $M^{2+}$ sites are occupied by Mg and Fe and one of the sites shows a greater preference for Fe than the other one.

Optically anisotropic sectors were observed also in the Mg-Zn solid solution (Fig. 3b) and the $Fe^{2+}$-Zn solid solution (Fig. 3a). Hence, ordering of the divalent cations can be seen in every solid solution studied here and is probably a common feature of the voltaite-pertlikite structures. Numerous attempts were undertaken to find out whether the anisotropic sectors are compositionally different from the isotropic portions of the crystals. The EDX line profiles in an electron microprobe showed no hints of elemental variations.

Optically anisotropic portions of crystals were seen, however, also in the end-members, for example in the sample Mn100 (Fig. 3c) or Zn100 (Fig. 3d). In this case, the anisotropic portions have the form of faint lamellae although the sample Mn100 shows anisotropic sectors similar to those in Mg80Zn20. These features will require further work but we can speculate that the anisotropy here is caused by ordering of $M^{2+}/Fe^{3+}$ over the octahedral sites. Such explanation could be especially true for Mn100 where we suspect a substantial mixing of $M^{2+}$ and $M^{3+}$ over the octahedral sites (see above). This explanation is further supported by the fact that the Fe100 crystals are completely isotropic. It is precisely these crystals where the least $M^{2+}/M^{3+}$ mixing was experimentally observed.

Anomalous anisotropy in other minerals

In the absence of a discernable chemical difference between the isotropic and anisotropic sectors, the question arises as to what triggers the symmetry change when the crystals grow. Anomalous optical anisotropy has been observed in other nominally cubic minerals, such as nabiasite (Brugger et al. 1999), pharmacosiderite (Zemann 1948; Buerger et al. 1967), more commonly in garnets, especially those from the ugrandite group (Allen and Buseck 1988), or in (Pb, Sr)$(NO_3)_2$ (Shtukenberg 2005). The anomalous behavior was usually explained by cation ordering, for example in garnets (Wildner and Andrut 2001; Shtukenberg et al. 2005) or (Pb,Sr)$(NO_3)_2$ (Shtukenberg 2005). For garnets, infrared spectra indicate also a non-cubic distribution of OH groups (Allen and Buseck 1988). Anomalous optical behavior is commonly observed also in diamonds, both natural (Rondeau et al. 2004) or synthetic (Shigley et al. 2005a, b; Welbourn et al. 2005) ones. The anisotropy is ascribed to the incorporation of N and H into the diamond structure and the strain induced by this incorporation, both for natural (Rondeau et al. 2004) and synthetic (Welbourn et al. 2005) diamonds. Furthermore, in synthetic diamonds color

variations are observed between the sectors which may be caused by incorporation of metals from the synthesis apparatus into different parts of the crystals.

It can be expected that many intermediate compositions found in nature have actually lower than the nominal symmetry, the latter usually determined for end-member or near-end-member compositions. Optical methods, however, are more sensitive than diffraction methods for detecting slight departures from nominal symmetry (Allen and Buseck 1988) and therefore, most of these deviations escape unnoticed. Unless the end-member is cubic, it is difficult to detect such changes even in an optical microscope.

We can only speculate that the coexistence of the cubic (voltaite) and tetragonal (pertlikite) phases in a single crystal may be a consequence of cation ordering on the growing crystal phases. The mechanisms which control the switch from one to the other are unknown. It is interesting that the innermost parts of our crystals are always cubic. Therefore, the nuclei are cubic and only further growth allows for the formation of the tetragonal sectors. Such consistent trends indicate perhaps that the nucleation and growth processes are different in some fundamental way. In addition, the voltaite crystals are noticeably large. If the growth was terminated early, either by stopping the experiment or by the intrinsic inability of the crystals to sustain their growth, tetragonal sectors would not develop.

**Table 5** Positions of bands in the infrared spectra of the end-member voltaite samples. The positions listed here were read as maxima of the features (bands or shoulders) in the spectra, not obtained by fitting these bands by mathematical functions

| Mn100 | Mg100 | Fe100 | Zn100 | $NH_4$-Mn | $NH_4$-Fe |
|---|---|---|---|---|---|
| 442 | 445 | 442 | 445 | 444 | 442 |
| 596 | 596 | 592 | 594 | 596 | 592 |
| 627 | 634 | 627 | 627 | 627 | 627 |
| 729 | 733 | 735 | 733 | 729 | 731 |
| 885 | 866 | 876 | 887 | 854 | 879 |
| 995 | 1014 | 1007 | 1007 | 1005 | 1007 |
| 1051 | 1065 | 1055 | 1053 | 1053 | 1055 |
| 1146 | 1182 | 1157 | 1124 | 1143 | 1130,1153 |
| | | | | 1431 | 1431 |
| 1639 | 1635 | 1630 | 1637 | 1641 | 1639 |
| 1686 | 1691 | 1687 | 1684 | 1686 | 1689 |
| 2497 | 2497 | 2499 | 2499 | 2501 | 2501 |
| 3111 | 3083 | 3074 | 3090 | 3114 | 3091 |
| 3379 | | 3417 | 3392 | 3261 | 3248 |
| | | | | 3379 | 3417 |
| | 3579 | 3558 | | 3560 | 3562 |

All data in $cm^{-1}$

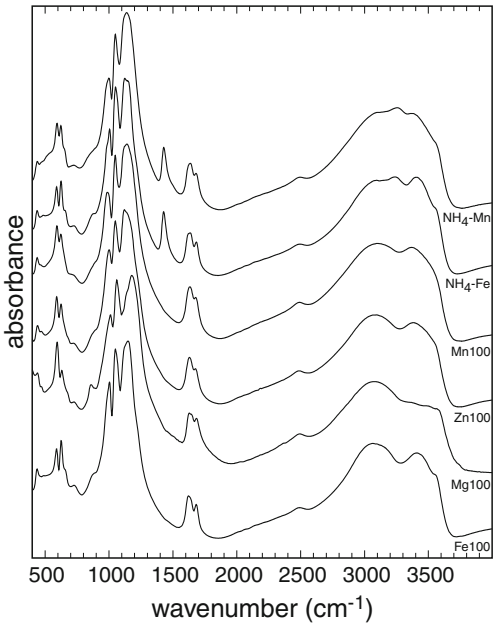


**Fig. 13** Infrared spectra of selected voltaite samples, marked with the sample codes (see Tables 1 and 2)

## Infrared spectroscopy

The mid-IR spectra of all voltaite samples are fairly similar (Table 5, Fig. 13). The only substantial difference is a band in the spectra of the $NH_4$-voltaite samples but such difference is expected. All samples show a broad set of features in a region characteristic for the stretching νOH vibrations. In the voltaite samples with $K^+$, this set consists of two broad bands located between 3,000 and 3,500 $cm^{-1}$. In some spectra, an additional shoulder at~3,560 $cm^{-1}$ is visible (see spectrum of Fe100 in Fig. 13). In the voltaite samples with $NH_4^+$, this set splits in three bands (see Table 5) owing to additional symmetric stretching vibrations of the $NH_4^+$ units in this range (Mookherjee et al. 2002). There is a weak, but consistently present band at ~2,500 $cm^{-1}$. The two bands between 1,600 and 1,700 $cm^{-1}$ can be assigned to H-O-H bending in the $H_2O$ molecules in voltaite. A sharp band at 1,431 $cm^{-1}$, visible only in the spectra of the $NH_4$-voltaite samples, arises from the asymmetric bending vibrations of the $NH_4^+$ group. The region between 1,000 and 1,200 $cm^{-1}$ is occupied by a series of strong bands which can be assigned to δOH bending and S-O stretching vibrations (Hertweck and Libowitzky 2002). The point symmetry of the single crystallographically distinct sulfate group in voltaite is $C_1$ and therefore, four $SO_4$ bands ($3\nu_3SO_4$ + $\nu_1SO_4$) are expected in the region between ~980 and 1,200 $cm^{-1}$. The $\nu_3SO_4$ band is assigned to asymmetric stretching and the $\nu_1SO_4$ band to symmetric stretching within the $SO_4$ group. In most of the data sets, only 3 bands were clearly resolved in this region, with hints of shoulders in some spectra.

**Acknowledgments** We are grateful to two anonymous reviewers for their constructive criticism. We thank D. Merten (Institute of Geosciences, Friedrich-Schiller-Universität Jena) for the ICP-OES analyses, H. Görls (Institute for Inorganic and Analytical Chemistry, Friedrich-Schiller-Universität Jena) for the single-crystal XRD data, G. Sentis (Institute of Pharmacy, Friedrich-Schiller-Universität Jena) for the infrared spectra, and B. Kreher-Hartmann (Institute of Geosciences, Friedrich-Schiller-Universität Jena) for the macrophotographs of the voltaite crystals. We acknowledge the ANKA Angströmquelle Karlsruhe for the provision of the beamtime at the PDIFF and SCD beamlines.

## References

Allen FM, Buseck PR (1988) XRD, FTIR, and TEM studies of optically anisotropic grossular garnets. Am Mineral 73:568–584

Beveridge D, Day P (1979) Charge transfer in mixed valence solids. Part 9. Preparation, characterization, and optical spectroscopy of the mixed valence mineral voltaite [aluminum pentairon(II) triiron (III) dipotassiumdodecasulfate 18-hydrate] and its solid solutions with cadmium(II). J Chem Soc Dalton Trans 4:648–653

Brugger J, Bonin M, Schenk KJ, Miesser N, Berlepsch P, Ragu A (1999) Description and crystal structure of nabiasite, $BaMn_9[(V, As)O_4]_6(OH)_2$, a new mineral from the Central Pyrénées (France). Eur J Mineral 11:879–890

Buerger MJ, Dollase WA, Garaycochea-Wittke I (1967) The structure and composition of the mineral pharmacosiderite. Z Kristallogr 125:92–108

Dahlman B (1952) The crystal structure of kroehnkite, $CuNa_2(SO_4)_2(H_2O)_2$ and brandtite, $MnCa_2(AsO_4)_2(H_2O)_2$. Ark Mineral Geol 1:339–366

Ertl A, Dyar MD, Hughes JH, Brandstatter F, Gunter ME, Prem M, Peterson RC (2008) Pertlikite, a new tetragonal Mg-rich member of the voltaite group from Madeni Zakh, Iran. Can Mineral 46:661–669

Fleck M, Kolitsch U, Hertweck B (2002) Natural and synthetic compounds with kröhnkite-type chains: review and classification. Z Kristallogr 217:435–443

Gieré R, Blackford M, Smith KL, Williams CT, Kirk C (2007) Metal sulfates in PM emissions from a coal-fired power plant. Goldschmidt conference abstracts, A322

Gossner B, Arm M (1930) Chemische und röntgenographische Untersuchung an Stoffen und Kristallen von komplexer Bauart. Z Kristallogr 72:202–236

Gossner B, Bäuerlein T (1933) Optical anomalies: voltaite-like sulfates. NJb Min Geol Pal 66A:1–40

Gossner B, Besslein J (1934) Hydrated sulfates of three metals. Centr Mineral Geol 1934A:358–364

Gossner B, Drexler K (1933) Structural and molecular units of sulfates of the voltaite type. Centr Mineral Geol 1933A:83–91

Gossner B, Fell E (1932) Sulfates of the voltaite type. Ber Deutsch Chem Ges 65B:393–395

Griffen DT, Ribbe PH (1979) Distortions in the tetrahedral oxyanions of crystalline substances. Neues Jahrb Miner Abh 137:54–73

Hawthorne FC, Krivovichev SV, Burns PC (2000) The crystal chemistry of sulfate minerals. Rev Mineral Geochem 40:1–112

Hermon E, Haddad R, Simkin D, Brandao DE, Muir WB (1976) Magnetic properties and the distribution of iron ions in voltaites. Can J Phys 54:1149–1156

Hertweck B, Libowitzky E (2002) Vibrational spectroscopy of phase transitions in leonite-type minerals. Eur J Mineral 14:1009–1017. doi:10.1127/0935-1221/2002/0014-1009

Jambor JL, Nordstrom DK, Alpers CN (2000) Metal-sulfate salts from sulfide mineral oxidation. Rev Mineral Geochem 40:303–350. doi:10.2138/rmg.2000.40.6

Long GJ, Longworth G, Day P, Beveridge D (1980) A Mössbauer-effect study of the electronic and magnetic properties of voltaite, a mixed-valence. Mineral Inorg Chem 19:821–829

Majzlan J, Alpers CN, Bender Koch C, McCleskey RB, Myneni SCB, Neil JM (2011) Vibrational, X-ray absorption, and Mössbauer spectra of sulfate minerals from the weathered massive sulfide deposit at Iron Mountain, California. Chem Geol 284:296–305

Marquez-Zavalia MF, Lomniczi de Upton I, Galliski MA (2001) Krausite in fumaroles from Santa Barbara mine, northwestern Argentina. Neues Jb Miner Monat 8:378–384

Mereiter K (1972) Die Kristallstruktur des Voltaits, $K_2Fe_5^{2+}Fe_3^{3+}Al[SO_4]_{12}\ 18H_2O$. Tschermaks Min Petr Mitt 18:185–202

Mookherjee M, Redfern SAT, Zhang M, Harlov DE (2002) Orientational order–disorder of $ND_4^+/NH_4^+$in synthetic $ND_4^+/NH_4^+$- phlogopite: a low-temperature infrared study. Eur J Mineral 14:1033–1039

Nordstrom DK, Alpers CN (1999) Negative pH, efflorescent mineralogy, and consequences for environmental restoration at the Iron Mountain. Proc Natl Acad Sci USA 96:3455–3462

Peterson RC, Valyashko E, Wang R (2009) The atomic structure of $(H_3O)Fe^{3+}(SO_4)_2$ and rhomboclase, $(H_5O_2)Fe^{3+}(SO_4)_2{\cdot}2H_2O$. Can Mineral 47:625–634

Rammelsberg CF (1860) Handbuch der Mineralchemie. Verlag von Wilhelm Engelman, Leipzig

Rondeau B, Fritsch E, Guiraud M, Chalain JP, Notari F (2004) Three historical 'asteriated' hydrogen-rich diamonds: growth history and sector-dependent impurity incorporation. Diam Relat Mater 13:1658–1673

Shannon RD (1976) Revised effective ionic radii and systematic studies of interatomic distances in halides and chalcogenides. Acta Crystallogr A32:751–767

Sheldrick G (2008) A short history of SHELX. Acta Crystallogr A64:112–122

Shigley JE, Fritsch E, Stockton CM, Koivula JI, Fryer CW, Kane RE (2005a) The gemological properties of the Sumitomo gem-quality synthetic yellow diamonds. In: Shigley JE (ed) Synthetic diamonds. Gems & Gemology in Review 30–45

Shigley JE, Fritsch E, Stockton CM, Koivula JI, Fryer CW, Kane RE, Hargett DR, Welch CW, (2005b) The gemological properties of the De Beers gem-quality synthetic diamonds. In: Shigley JE (ed) Synthetic diamonds. Gems & Gemology in Review 46–64

Shtukenberg AG (2005) Metastability of atomic ordering in lead-strontium nitrate solid solutions. J Solid State Chem 178:2608–2612

Shtukenberg AG, Popov DY, Punin YO (2005) Growth ordering and anomalous birefringence in ugrandite garnets. Mineral Mag 69:537–550

Stracher GB, Prakash A, Schroeder P, McCormack J, Zhang X, Van Dijk P, Blake D (2005) New mineral occurrences and mineralization processes: Wuda coal-fire gas vents of Inner Mongolia. Am Mineral 90:1729–1739

Welbourn CM, Cooper M, Spear PM (2005) De Beers natural versus synthetic diamond verification instruments. In: Shigley JE (ed) Synthetic diamonds. Gems & Gemology in Review 139–151

Wildner M, Andrut M (2001) The crystal chemistry of birefringent natural uvarovites: Part II. Single-crystal X-ray structures. Am Mineral 86:1231–1251

Zavalia MFM, Galliski MA (1995) Goldichite of fumarolic origin from the Santa Barbara mine, Jujuy, northwestern Argentina. Can Mineral 33:1059–1062

Zemann J (1948) Formel und Strukturtyp des Pharmakosiderits. Tschermaks Min Petr Mitt 1:1–13